

Five-wave-packet quantum error correction based on continuous-variable cluster entanglement

Shuhong Hao, Xiaolong Su,* and Caixing Tian, Changde Xie and Kunchi Peng

*State Key Laboratory of Quantum Optics and Quantum Optics Devices,
Institute of Opto-Electronics, Shanxi University, Taiyuan, 030006, People's Republic of China*

Quantum error correction protects the quantum state against noise and decoherence in quantum communication and quantum computation, which enables one to perform fault-tolerant quantum information processing. We experimentally demonstrate a quantum error correction scheme with a five-wave-packet code against a single stochastic error, the original theoretical model of which is firstly proposed by S. L. Braunstein and T. A. Walker. Five submodes of a continuous variable cluster entangled state of light are used for five encoding channels. Especially, in our encoding scheme the information of the input state is only distributed on three of the five channels and thus any error appearing in the remained two channels never affects the output state, i.e. the output quantum state is immune from the error in the two channels. The stochastic error on a single channel is corrected for both vacuum and squeezed input states and the achieved fidelities of the output states are beyond the corresponding classical limit.

PACS numbers: 03.67.Pp, 03.67.Hk, 42.50.Dv, 42.50.-p

I. INTRODUCTION

The transmission of quantum states with high fidelity is an essential requirement for implementing quantum information processing with high quality. However, losses and noises in channels inevitably lead to errors into transmitted quantum states and thus make the distortion of resultant states. The aim of quantum error correction (QEC) is to eliminate or, at least, reduce the hazards resulting from the imperfect channels and to ensure transmission of quantum states with high fidelity [1]. A variety of discrete variable QEC protocols, such as nine-qubit code [2], five-qubit code [3], topological code [4, 5], have been suggested and the experiments of QEC have been realized in different physical systems, such as nuclear magnetic resonance [6–8], ionic [9, 10], photonic [11, 12], superconducting systems [13, 14] and Rydberg atoms [15].

Besides quantum information with discrete variables, quantum information with continuous variables (CV) is also promptly developing [16–23]. Different types of CV QEC codes for correcting single non-Gaussian error have been proposed, such as nine-wave-packet code [24, 25], five-wave-packet code [26, 27], entanglement-assisted code [28] and erasure-correcting code [29]. A CV QEC scheme against Gaussian noise with a non-Gaussian operation of photon counting has been also theoretically analyzed [30]. The CV QEC schemes of the nine-wave-packet code [31], erasure-correcting code against photon loss [32] and the correcting code with the correlated noisy channels [33] have been experimentally demonstrated.

According to the no-go theorem proved in Ref. [34], Gaussian errors are impossible to be corrected with pure Gaussian operations. However, non-Gaussian stochas-

tic errors, which frequently occur in free-space channels with atmospheric fluctuations for example [35–37], can be corrected by Gaussian schemes since the no-go theorem does not apply in this case. Generally, the stochastic error model is described by [38]

$$W_{out}(x, p) = (1 - \gamma)W_{in}(x, p) + \gamma W_{error}(x, p), \quad (1)$$

where the input state $W_{in}(x, p)$ is transformed into a new state $W_{error}(x, p)$ with probability γ or it remains unchanged with probability $1 - \gamma$. Even for the case of two Gaussian states $W_{in}(x, p)$ and $W_{error}(x, p)$, the output state $W_{out}(x, p)$ is also non-Gaussian, that is, this channel model describes a certain, simple form of non-Gaussian errors.

In 2009 T. Aoki et al. presented the first experimental implementation of a Shor-type nine-channel QEC code based on entanglement among nine optical beams, which was the achievable largest entangled state on experiments then [31]. This scheme is deterministically implemented using only linear operations and resources, which can correct arbitrary single beam error. Although S. L. Braunstein discovered a highly efficient five-wave-packet code theoretically in 1998, its linear optical construction was not proposed [26]. Later, in 2010, T. A. Walker and S. L. Braunstein outlined a new approach for generating linear optics circuits that encode QEC code and proposed a linear optics construction for a five-wave-packet QEC code [27]. Differentiating from previous approaches by means of directly transferring existing qubit codes into CV codes, they defined the conditions for yielding a CV QEC code firstly and then searched numerically for circuits satisfying this criterion. The five-wave-packet code improves on the capacity of the best known code implemented by linear optics and saturates the lower bound for the number of carrier needed for a single-error-correct code [27]. However, the proposed five-wave-packet CV QEC code has not been experimentally demonstrated so far.

*Electronic address: suxl@sxu.edu.cn

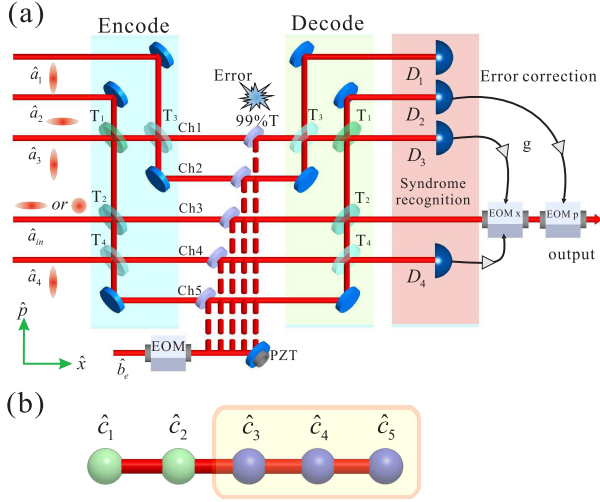


FIG. 1: (color online) The schematic of the QEC scheme. (a): the schematic of experimental set-up. PZT: piezoelectric transducer. EOM: electro-optical modulator, T_{1-4} : beam-splitters with 25%, 33%, 50%, and 50% transmission, respectively. Ch1-5: quantum channels. 99%T: a beam-splitter with 99% transmission. D_1 - D_4 : homodyne detectors, g : gain in the feedforward circuit. (b): the graph representation of the five-wave-packet code. The input state is encoded on submodes \hat{c}_3 , \hat{c}_4 and \hat{c}_5 of a five-partite linear cluster state \hat{c}_{1-5} .

Based on the approach outlined by T. A. Walker and S. L. Braunstein [27], we design a more compact linear optics construction and achieve the first experimental demonstration of five-wave-packet CV QEC code using a five-partite CV cluster entangled state [39, 40]. In this experiment only four ancilla squeezed states of light are required and four optical beamsplitters are used in the encoding and the decoding system, respectively. Comparing with the nine-wave-packet system [31], the required quantum resources and utilized optical elements in our system decrease a half. The smaller codes not only save quantum resources, but also increase data rates and decrease the chance of further occurring errors, thus are very significant for the development of quantum information technology [27]. In the presented encoding method, only a part of all wave packets (three of five in the presented experiment) involves the information of the input state and therefore the noise occurring in the remained channels (channels 1 and 2 in the presented system) do not introduce any error into the transmitted quantum state. Such that, we do not need to perform the error correction for the remained channels and the near unity fidelity is achieved in these channels. We name the encoding method as the partial encoding. It should be emphasized that although the remained two channels do not involve the information of the input state, they play the unabsolvable roles in the syndrome recognition and the error correction. In the presented QEC experiment, the error correction is implemented in a deterministic fashion due to the application of unconditional CV quantum

entanglement [16, 17]. A vacuum state and a squeezed vacuum state are utilized as the input states, respectively, to exhibit the QEC ability of the system for different input states. According to the standard notation for QEC code [1], the presented five-wave-packet code should be expressed by $[n, k, d] = [5, 1, 3]$, where $n = 5$ denote the number of used wave packets, $k = 1$ is the number of logical encoded input state, and $d = 3$ is the distance, which indicates how many errors can be tolerated, a code of distance d can correct up to $(d - 1)/2$ arbitrary errors at unspecified channels.

II. RESULTS

A. Encoding.

The schematic of the CV QEC scheme is shown in Figure 1(a). The QEC procedure contains five stages, which are encoding, error-in, decoding, syndrome recognition and correction, respectively. The encoding is completed by a beam-splitter network consisting of four beam-splitters (T_1 - T_4). Four squeezed states with -3.5 dB squeezing (\hat{a}_{1-4}) generated by three non-degenerate optical parametric amplifiers, are used as ancilla modes (see APPENDIX A for details). In the experiment, three amplitude-squeezed states, $\hat{a}_m = e^{-r}\hat{x}_m^{(0)} + ie^{+r}\hat{p}_m^{(0)}$ ($m = 1, 3, 4$), and a phase-squeezed state, $\hat{a}_n = e^{+r}\hat{x}_n^{(0)} + ie^{-r}\hat{p}_n^{(0)}$ ($n = 2$) are applied, where r is the squeezing parameter ($r = 0$ and $r = +\infty$ correspond to no squeezing and perfect squeezing, respectively), $\hat{x}_j^{(0)}$ and $\hat{p}_j^{(0)}$ denote the amplitude and phase quadratures of the vacuum field, respectively. The transformation matrix of the encoding network is expressed by

$$U = \begin{pmatrix} \frac{1}{\sqrt{2}} & \frac{\sqrt{3}}{2\sqrt{2}} & \frac{1}{2\sqrt{2}} & 0 & 0 \\ \frac{1}{\sqrt{2}} & \frac{-1}{2\sqrt{2}} & \frac{1}{2\sqrt{2}} & 0 & 0 \\ 0 & \frac{1}{\sqrt{6}} & \frac{-1}{\sqrt{2}} & \frac{1}{\sqrt{3}} & 0 \\ 0 & \frac{1}{2\sqrt{6}} & \frac{-1}{2\sqrt{2}} & \frac{\sqrt{3}}{\sqrt{3}} & \frac{1}{\sqrt{2}} \\ 0 & \frac{-1}{2\sqrt{6}} & \frac{1}{2\sqrt{2}} & \frac{1}{\sqrt{3}} & \frac{1}{\sqrt{2}} \end{pmatrix}. \quad (2)$$

The unitary matrix can be decomposed by $U = B_{45}^-(1/2)B_{34}^+(1/3)B_{12}^+(1/2)B_{23}^+(1/4)$. Here, $B_{kl}^\pm(T)$ stands for the transformation of modes k and l on a beam-splitter, the corresponding transformation matrix is given by

$$B^\pm = \begin{pmatrix} \sqrt{1-T} & \sqrt{T} \\ \pm\sqrt{T} & \mp\sqrt{1-T} \end{pmatrix}. \quad (3)$$

The input state \hat{a}_{in} is encoded with the four ancilla modes by $(\hat{c}_1, \hat{c}_2, \hat{c}_3, \hat{c}_4, \hat{c}_5)^T = U(\hat{a}_1, \hat{a}_2, \hat{a}_3, \hat{a}_{in}, \hat{a}_4)^T$.

The encoded five modes are

$$\begin{aligned}
\hat{c}_1 &= \frac{\hat{a}_1}{\sqrt{2}} + \frac{\sqrt{3}\hat{a}_2}{2\sqrt{2}} + \frac{\hat{a}_3}{2\sqrt{2}}, \\
\hat{c}_2 &= \frac{\hat{a}_1}{\sqrt{2}} - \frac{\sqrt{3}\hat{a}_2}{2\sqrt{2}} - \frac{\hat{a}_3}{2\sqrt{2}}, \\
\hat{c}_3 &= \frac{\hat{a}_2}{\sqrt{6}} - \frac{\hat{a}_3}{\sqrt{2}} + \frac{\hat{a}_{in}}{\sqrt{3}}, \\
\hat{c}_4 &= \frac{\hat{a}_2}{2\sqrt{6}} - \frac{\hat{a}_3}{2\sqrt{2}} + \frac{\hat{a}_4}{\sqrt{2}} - \frac{\hat{a}_{in}}{\sqrt{3}}, \\
\hat{c}_5 &= \frac{-\hat{a}_2}{2\sqrt{6}} + \frac{\hat{a}_3}{2\sqrt{2}} + \frac{\hat{a}_4}{\sqrt{2}} + \frac{\hat{a}_{in}}{\sqrt{3}}.
\end{aligned} \tag{4}$$

From equation (4) we can see, the input state is partially encoded on channels 3, 4 and 5 (\hat{c}_3 , \hat{c}_4 and \hat{c}_5) by means of the designed beam-splitter network, while the encoded states in channels 1 and 2 (\hat{c}_1 and \hat{c}_2) do not contain any information of the input state.

As shown in Figure 1(b) the encoded five modes \hat{c}_i ($i = 1, \dots, 5$) is the five submodes of a five-partite CV linear cluster entangled state [39, 40]. The correlation noises of quadrature components among the encoded five wave-packets are expressed by $\hat{x}_{c1} + \hat{x}_{c2} = \sqrt{2}\hat{x}_1^{(0)}e^{-r}$, $\hat{p}_{c2} - \hat{p}_{c1} - \hat{p}_{c3} = (-2\sqrt{2}\hat{p}_2^{(0)}e^{-r} - \hat{p}_{in})/\sqrt{3}$, $\hat{x}_{c3} + \hat{x}_{c2} + \hat{x}_{c4} = (\hat{x}_1^{(0)}e^{-r} - 2\hat{x}_3^{(0)}e^{-r} + \hat{x}_4^{(0)}e^{-r})/\sqrt{2}$, $\hat{p}_{c4} - \hat{p}_{c3} - \hat{p}_{c5} = -\sqrt{3}\hat{p}_{in}$, and $\hat{x}_{c4} + \hat{x}_{c5} = \sqrt{2}\hat{x}_4^{(0)}e^{-r}$. These expressions show that the correlation noises of $\hat{x}_{c1} + \hat{x}_{c2}$, $\hat{x}_{c3} + \hat{x}_{c2} + \hat{x}_{c4}$ and $\hat{x}_{c4} + \hat{x}_{c5}$ are smaller than the corresponding normalized shot-noise-level (SNL) for any non-zero squeezing of the ancilla modes. While the correlation noises of $\hat{p}_{c2} - \hat{p}_{c1} - \hat{p}_{c3}$ and $\hat{p}_{c4} - \hat{p}_{c3} - \hat{p}_{c5}$ depend on the input state, i.e. they have different values for different input state. The inseparability criteria of the five-mode cluster entangled state are denoted by [41]

$$\begin{aligned}
\langle \Delta(\hat{x}_{c1} + \hat{x}_{c2})^2 \rangle + \langle \Delta(\hat{p}_{c2} - \hat{p}_{c1} - \hat{p}_{c3})^2 \rangle &< 1, \\
\langle \Delta(\hat{p}_{c2} - \hat{p}_{c1} - \hat{p}_{c3})^2 \rangle + \langle \Delta(\hat{x}_{c3} + \hat{x}_{c2} + \hat{x}_{c4})^2 \rangle &< 1, \\
\langle \Delta(\hat{x}_{c3} + \hat{x}_{c2} + \hat{x}_{c4})^2 \rangle + \langle \Delta(\hat{p}_{c4} - \hat{p}_{c3} - \hat{p}_{c5})^2 \rangle &< 1, \\
\langle \Delta(\hat{p}_{c4} - \hat{p}_{c3} - \hat{p}_{c5})^2 \rangle + \langle \Delta(\hat{x}_{c4} + \hat{x}_{c5})^2 \rangle &< 1.
\end{aligned} \tag{5}$$

When all combinations of correlation variances on the left of the inequalities (5) are less than the normalized boundary on the right side, the five-wave-packet optical state is a CV cluster entangled state. With a vacuum input state and choosing the optimal gains of g_i ($i = 1, 2, \dots, 6$) the inseparability criteria will be satisfied for any non-zero squeezing of the ancilla modes. In this case, the encoded five wave packets form a five-partite linear cluster entangled state.

B. Error-in.

The five encoded wave packets constitute five quantum channels, where the errors possibly occur. In the

experiment, the noise is modulated on an excess optical beam (\hat{b}_e) by an electro-optical modulator (EOM) drove by a sin-wave signal at 2 MHz to make an error beam firstly. Then, the error beam is randomly coupled into any one of the five coded wave packets each time by a mirror of 99% transmission. By sweeping the phase of the error wave packet with the piezoelectric translator (PZT) attached on a reflection mirror, a quasi-random displacement error is added on one of the five channels. The experimental operation corresponds to adding an error operator \hat{e}_i ($i = 1, 2, \dots, 5$) on a corresponding optical wave packet, the mathematic expression of which is $U(\hat{a}_1, \hat{a}_2, \hat{a}_3, \hat{a}_{in}, \hat{a}_4)^T + (\hat{e}_1, \hat{e}_2, \hat{e}_3, \hat{e}_4, \hat{e}_5)^T$, where only one of \hat{e}_i is non-zero when an error is occurring in one channel.

C. Decoding.

The decoding circuit is the inverse of the encoding circuit. After decoding, the output mode (\hat{d}_{out}) and syndrome modes (\hat{d}_1 , \hat{d}_2 , \hat{d}_3 and \hat{d}_4) of the five channels are calculated by $U^{-1}[U(\hat{a}_1, \hat{a}_2, \hat{a}_3, \hat{a}_{in}, \hat{a}_4)^T + (\hat{e}_1, \hat{e}_2, \hat{e}_3, \hat{e}_4, \hat{e}_5)^T]$. The decoded modes are

$$\begin{aligned}
\hat{d}_1 &= \hat{a}_1 + \frac{\hat{e}_1 + \hat{e}_2}{\sqrt{2}}, \\
\hat{d}_2 &= \hat{a}_2 + \frac{3\hat{e}_1 - 3\hat{e}_2 + 2\hat{e}_3 + \hat{e}_4 - \hat{e}_5}{2\sqrt{6}}, \\
\hat{d}_3 &= \hat{a}_3 + \frac{\hat{e}_1 - \hat{e}_2 - 2\hat{e}_3 - \hat{e}_4 + \hat{e}_5}{2\sqrt{2}}, \\
\hat{d}_{out} &= \hat{a}_{in} + \frac{\hat{e}_3 - \hat{e}_4 + \hat{e}_5}{\sqrt{3}}, \\
\hat{d}_4 &= \hat{a}_4 + \frac{\hat{e}_4 + \hat{e}_5}{\sqrt{2}}.
\end{aligned} \tag{6}$$

It is obvious that the input state and ancilla modes are recovered after the decoding stage and the errors are included in five output channels. Please note that the output state \hat{d}_{out} does not contain the errors \hat{e}_1 and \hat{e}_2 , which means that the output state is immune from errors in channels 1 and 2. If the error occurs in channels 1 and 2, the output state will not be affected.

D. Syndrome measurement.

From the decoded modes, we can see that the error in different channels results in different outputs of the homodyne detectors D₁-D₄. By the DC outputs of the homodyne detectors, we can determine in which channel the error is occurring (see Table 1). If a syndrome mode does not contain the error in a certain channel, the DC output of the corresponding detector will be a straight line without any fluctuation. When the error appearing in a syndrome mode, the DC output of the corresponding detector will be a line with fluctuation (coming from

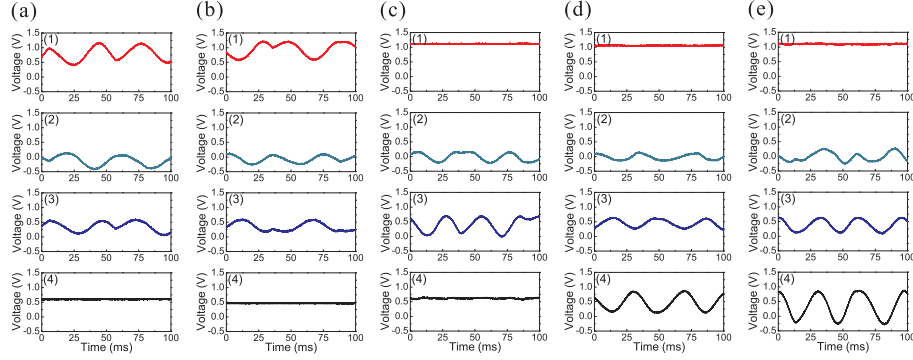


FIG. 2: (color online) Error syndrome measurement results. (a)-(e) correspond to that a random displacement error is imposed on channel 1-5, respectively. The DC outputs of detectors D1-D4 are recorded by a four-channel digital oscilloscope and the results are shown in (1)-(4) from top to bottom, respectively.

Table 1 Error syndrome measurements.

The error channel	Detectors with fluctuation	Measurement basis
1	1, 3 (in-phase)	x
	2	p
2	1, 3 (out-of-phase)	x
	2	p
3	3	x
	2	p
4	3, 4 (out-of-phase)	x
	2	p
5	3, 4 (in-phase)	x
	2	p

the error). A four-channel digital oscilloscope is used to record the DC output of detectors D₁-D₄. Figure 2 shows error syndrome measurement results. In Figure 2(a), outputs with fluctuation are obtained by detectors D₁, D₂ and D₃, and the fluctuations of detectors D₁ and D₃ are in-phase. The output of D₄ is a straight line because the syndrome mode \hat{a}_4 does not contain the error in channel 1 (\hat{e}_1). Comparing this result with table 1, we can identify that an error is occurring in channel 1. In Figure 2(b), we have outputs with fluctuation for detectors D₁, D₂ and D₃, and the outputs of detectors D₁ and D₃ are out-of-phase, which means that an error is occurring in channel 2. With the same way, we know that the error occurs in channels 3, 4 and 5 from the measured results in Figure 2(c), 2(d) and 2(e), respectively.

E. Error-correction.

After the position of the error is identified, we can correct the error by feedforwarding the measurement results of the corresponding homodyne detectors D₁-D₄ to the output state with suitable gains (see Table 2). The partial encoding method simplifies the error correction pro-

cedure. When the error is occurring in channels 1 and 2, we do not need to correct it because it does not affect the output state. When the error occurs in the channel 3, 4 or 5, the output state will be stained by the error and we need to implement the feedforward of the measurement results.

Figure 3 shows the results of QEC procedure for a vacuum input. The correction results for an error occurring in channels 1-5 are shown in Figure 3(a)-3(e), respectively. The quadrature components of output states before the error correction (cyan line), and after the correction (red and blue line) are given, where the red and blue lines correspond to the case using the squeezed and coherent state to be the ancilla modes, respectively, the black lines are the SNL. From Figure 3(a) and 3(b), we can see that the output state is immune from errors appearing in channels 1 and 2. Thus, we do not need to perform error correction when errors are occurring in channels 1 and 2. When the error is imposed on channels 3, 4 and 5, the output state contains the error signal before the error correction [cyan lines in Figure 3(c), 3(d) and 3(e)]. In the error correction procedure, the measurement results of detectors 3 (or 4) and 2 are feedforward to the output state (see Table 2). Figure 3(c)-3(e) show, when the squeezed ancilla modes are utilized, the noises on the output state are reduced. The better the squeezing, the lower the noise of output state. When the used ancilla modes are perfect squeezed states, the output state will totally overlap with the input vacuum state. The measured noise power of the output state can be found in APPENDIX C.

QEC results with a phase-squeezed state (-3.5 dB / 8.9 dB squeezing/antisqueezing) as the input state are shown in Figure 4. Figure 4(a)-4(e) are the results of the corrections for an error in channels 1-5, respectively. In Figure 4(a) and 4(b), the output state is still a phase squeezed state before the error correction (cyan line) when errors are occurring in channels 1 and 2, which shows that the output state is not affected by errors in channels 1 and 2. The measured squeezing and anti-

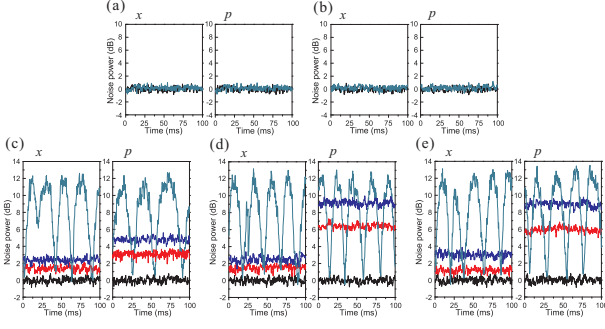


FIG. 3: (color online) The error correction results for a vacuum input. (a)-(e) are the results of error correction with an error on channel 1-5, respectively. Black lines: the SNL. Cyan lines: the noises on amplitude (x) and phase (p) components of output state before error correction. Blue and red lines are the noises on x and p components of output state with the coherent and squeezed ancilla modes, respectively. Measurement frequency is 2 MHz, the spectrum analyzer resolution bandwidth is 30 kHz, and the video bandwidth is 300 Hz.

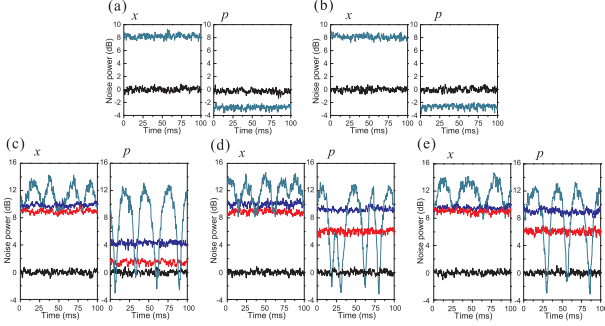


FIG. 4: (color online) The error correction results for a phase-squeezed input. (a)-(e) are the results of error correction with an error on channel 1-5, respectively. Black lines: the SNL. Cyan lines: the noises of the amplitude (x) and phase (p) components of output state before the error correction. Blue and red lines correspond to the noises levels of output state after the error correction with the coherent and squeezed ancilla modes, respectively. Measurement frequency is 2 MHz, the spectrum analyzer resolution bandwidth is 30 kHz, and the video bandwidth is 300 Hz.

squeezing of the output state are -2.78 dB / 8.22 dB and -2.73 dB / 8.09 dB for the errors in channels 1 and 2, respectively. The decrease of the squeezing derives from the imperfection in the experiment, such as channel loss and fluctuation of phase locking system. When the error is imposed on channel 3, 4 and 5, the output state becomes very noisy before error correction (cyan line). After error correction, the measured noise of the output state with the squeezed ancilla modes (red line) is below that using coherent states as the ancilla modes (blue line).

The fidelity $F = \{\text{Tr}[(\sqrt{\hat{\rho}_1}\hat{\rho}_2\sqrt{\hat{\rho}_1})^{1/2}]\}^2$, which denotes the overlap between the experimentally obtained

Table 2 Error correction feedforward components and the obtained fidelities.

Error in channel	Quadrature of output	Feedforward components	Fidelity with coherent state	Fidelity with squeezing
1	x	0	0.99 (0.99)	0.99 (0.99)
	p	0		
2	x	0	0.99 (0.99)	0.99 (0.99)
	p	0		
3	x	$\sqrt{2/3}x_3$	0.60 (0.68)	0.75 (0.85)
	p	$-\sqrt{2}p_2$		
4	x	$\sqrt{2/3}x_4$	0.40 (0.42)	0.56 (0.60)
	p	$2\sqrt{2}p_2$		
5	x	$-\sqrt{2/3}x_4$	0.39 (0.44)	0.59 (0.59)
	p	$2\sqrt{2}p_2$		

Fidelities in and out of brackets are for the case of a squeezed and a vacuum state used as input state, respectively.

output state $\hat{\rho}_2$ and the input state $\hat{\rho}_1$, is utilized to quantify the performance of the QEC code. The fidelity for two Gaussian states $\hat{\rho}_1$ and $\hat{\rho}_2$ with the covariance matrices σ_j is expressed by [42, 43]

$$F = \frac{2}{\sqrt{\Delta + \sigma} - \sqrt{\sigma}} \exp[-\beta^T(\sigma_1 + \sigma_2)^{-1}\beta], \quad (7)$$

where $\Delta = \det(\sigma_1 + \sigma_2)$, $\sigma = (\det \sigma_1 - 1)(\det \sigma_2 - 1)$, $\beta = \alpha_2 - \alpha_1$, and α_j is the mean amplitudes $\alpha_j \equiv (\alpha_{jx}, \alpha_{jp})^T$ ($j = 1, 2$), σ_1 and σ_2 are the covariance matrices for the input state ($\hat{\rho}_1$) and the experimentally obtained output state ($\hat{\rho}_2$), respectively. In our experiment, a vacuum state and a squeezed vacuum state are used for the input states, respectively, and the mean amplitude for the both states equals to zero. If squeezed states with infinite squeezing ($r \rightarrow \infty$) are utilized as the ancilla states, the fidelity will equal to 1. When all ancilla modes are the coherent states of light with zero classical noise ($r = 0$), the obtained fidelity of the output state is the corresponding classical limit [31, 32]. Since the errors in channels 1 and 2 do not affect the output state, the obtained fidelity is near unity (0.99). The fidelity obtained with squeezed states to be the ancilla modes is higher than that obtained with coherent states when error appears in channel 3, 4 and 5 (see Table 2).

III. DISCUSSION

The presented compact five-wave-packet QEC code can be applied to correct a single stochastic error in a single quantum channel. For this type of error correction one usually assume that errors occur stochastically with a small probability so that multiple errors are unlikely to happen. When two or more errors are occurring simultaneously on the encoded channels, the errors can not be

identified and corrected because the syndrome measurement will be confusing [31, 32].

The general error $\hat{e} = \hat{x} + i\hat{p}$ ($\hat{x} \neq 0$, $\hat{p} \neq 0$) and x -displacement error $\hat{e} = \hat{x}$ can be well recognized and corrected suitably with the presented scheme. For the p -displacement error $\hat{e} = i\hat{p}$, it is unclear which channel the error comes from since only the phase measurement of detector D₂ has output with fluctuation for all five channels (see Table 1). If this happens in the syndrome measurement results, we need to apply a Fourier transformation F (a 90° rotation in the phase space) on each ancilla mode in the encoding stage. In this way, the output state is given by $U^{-1}[U(F\hat{a}_1, F\hat{a}_2, F\hat{a}_3, \hat{a}_{in}, F\hat{a}_4)^T + (\hat{e}_1, \hat{e}_2, \hat{e}_3, \hat{e}_4, \hat{e}_5)^T] = (F\hat{a}_1, F\hat{a}_2, F\hat{a}_3, \hat{a}_{in}, F\hat{a}_4)^T + U^{-1}(\hat{e}_1, \hat{e}_2, \hat{e}_3, \hat{e}_4, \hat{e}_5)^T$ and thus in the syndrome stage, the amplitude quadrature of detector D₂ and phase quadratures of detectors D₁, D₃, D₄ are measured. Such that, the p -displacement error can be identified by the outputs with fluctuation from detectors D₁, D₃ and D₄.

In summary, we experimentally demonstrated a compact five-wave-packet CV QEC code using a five-partite cluster entangled state of light. The QEC code is implemented only with linear optics operations and four ancilla squeezed states of light. The compact optics circuit can increase data rates and decrease chance of further error occurring. The presented partial encoding method may simplify the error correction procedure and improve the efficiency of QEC. The presented experiment is the first experimental demonstration of the approach proposed by S. L. Braunstein and T. A. Walker for designing linear optics circuits of CV QEC code, which has potential application in constructing future CV quantum information networks.

Acknowledgements

This research was supported by the National Basic Research Program of China (Grant No. 2010CB923103), NSFC (Grant Nos. 11174188, 61475092) and OIT.

APPENDIX

A. Experimental details

The amplitude-squeezed and phase-squeezed states are produced by three non-degenerate optical parametric amplifiers (NOPAs) with identical configuration. These NOPAs are pumped by a common laser source, which is a continuous wave intracavity frequency-doubled and frequency-stabilized Nd:YAP/LBO(Nd-doped YAlO₃ perovskite/lithium triborate) laser [44]. Each of NOPAs consists of an α -cut type-II KTP crystal and a concave mirror [45]. The front face of the KTP is coated to be used for the input coupler and the concave mirror serves as the output coupler of the squeezed states.

The transmissions of the input coupler at 540 nm and 1080 nm are 99.8% and 0.04%, respectively. The transmissions of the output coupler at 540 nm and 1080 nm are 0.5% and 5.2%, respectively. An NOPA simultaneously generates an amplitude-squeezed state and a phase-squeezed state in two orthogonal polarizations [46]. The ancilla modes \hat{a}_1 , \hat{a}_2 and \hat{a}_3 , \hat{a}_4 and the phase-squeezed input state, are generated by three NOPAs respectively. Three NOPAs are locked individually by using Pound-Drever-Hall method with a phase modulation of 56 MHz on 1080 nm laser beam. All NOPAs are operated at deamplification condition, which corresponds to lock the relative phase between the pump laser and the injected signal to $(2n+1)\pi$ (n is the integer).

The transmission efficiency of an optical beam from NOPA to a homodyne detector is around 96%. The quantum efficiency of a photodiode (FD500W-1064, Fermionics) used in the homodyne detection system is 95%. The interference efficiency on a beam-splitter is about 99%.

The Fourier transformation F needed for the correction of p -displacement error is a 90° rotation in the phase space, which changes the squeezing direction of the squeezed state. The Fourier transformations on the ancilla modes \hat{a}_1 and \hat{a}_4 can be completed by changing the relative phase difference on the beam-splitters T₃ and T₄ from 0 to $\pi/2$, respectively. The Fourier transformations on the ancilla modes \hat{a}_2 and \hat{a}_3 can be implemented by exchanging the position of \hat{a}_2 and \hat{a}_3 on the beam-splitter T₁, which can be simply achieved by rotating the half wave-plate for 45° placed at the output port of the NOPA that is because \hat{a}_2 and \hat{a}_3 are produced from one NOPA [46].

B. Details of syndrome and error-correction procedure

When the error is occurring in channel 1, we have non-zero syndrome measurement for

$$\begin{aligned}\hat{x}_{D1} &= \frac{\hat{x}_{e1}}{\sqrt{2}} + \hat{x}_1^{(0)}e^{-r}, \\ \hat{x}_{D3} &= \frac{\hat{x}_{e1}}{2\sqrt{2}} + \hat{x}_3^{(0)}e^{-r}, \\ \hat{p}_{D2} &= \frac{3\hat{p}_{e1}}{2\sqrt{6}} + \hat{p}_2^{(0)}e^{-r},\end{aligned}\quad (8)$$

where the outputs of \hat{x}_{D1} and \hat{x}_{D3} are in-phase. At this case, the output state is

$$\begin{aligned}\hat{x}_{out} &= \hat{x}_{in}, \\ \hat{p}_{out} &= \hat{p}_{in},\end{aligned}\quad (9)$$

which is immune from the error in channel 1, thus we do not need any correction.

When the error is occurring in channel 2, non-zero syn-

drome measurement is obtained for

$$\begin{aligned}\hat{x}_{D1} &= \frac{\hat{x}_{e2}}{\sqrt{2}} + \hat{x}_1^{(0)} e^{-r}, \\ \hat{x}_{D3} &= \frac{-\hat{x}_{e2}}{2\sqrt{2}} + \hat{x}_3^{(0)} e^{-r}, \\ \hat{p}_{D2} &= \frac{-3\hat{p}_{e2}}{2\sqrt{6}} + \hat{p}_2^{(0)} e^{-r},\end{aligned}\quad (10)$$

where \hat{x}_{D1} and \hat{x}_{D3} are out-of-phase. The corresponding output state is

$$\begin{aligned}\hat{x}_{out} &= \hat{x}_{in}, \\ \hat{p}_{out} &= \hat{p}_{in},\end{aligned}\quad (11)$$

and we do not need any correction.

When the error is occurring in channel 3, non-zero syndrome measurements are obtained for

$$\begin{aligned}\hat{x}_{D3} &= \frac{-2\hat{x}_{e3}}{2\sqrt{2}} + \hat{x}_3^{(0)} e^{-r}, \\ \hat{p}_{D2} &= \frac{2\hat{p}_{e3}}{2\sqrt{6}} + \hat{p}_2^{(0)} e^{-r}.\end{aligned}\quad (12)$$

In this case, the output state is

$$\begin{aligned}\hat{x}_{out} &= \hat{x}_{in} + \frac{\hat{x}_{e3}}{\sqrt{3}}, \\ \hat{p}_{out} &= \hat{p}_{in} + \frac{\hat{p}_{e3}}{\sqrt{3}}.\end{aligned}\quad (13)$$

To eliminate the error, $\frac{\sqrt{2}}{\sqrt{3}}\hat{x}_{D3}$ and $-\sqrt{2}\hat{p}_{D2}$ should be fedforward to \hat{x}_{out} and \hat{p}_{out} , respectively. The corrected output mode is given by

$$\begin{aligned}\hat{x}'_{out} &= \hat{x}_{in} + \frac{\sqrt{2}}{\sqrt{3}}\hat{x}_3^{(0)} e^{-r}, \\ \hat{p}'_{out} &= \hat{p}_{in} - \sqrt{2}\hat{p}_2^{(0)} e^{-r}.\end{aligned}\quad (14)$$

The noise powers of the output state are

$$\langle \Delta^2 \hat{x}'_{out} \rangle = \langle \Delta^2 \hat{x}_{in} \rangle + \frac{2}{3} \times \frac{1}{4} e^{-2r} \quad (15)$$

and

$$\langle \Delta^2 \hat{p}'_{out} \rangle = \langle \Delta^2 \hat{p}_{in} \rangle + 2 \times \frac{1}{4} e^{-2r}, \quad (16)$$

respectively.

When the error is occurring in channel 4, we have non-zero syndrome measurements on

$$\begin{aligned}\hat{x}_{D3} &= \frac{-\hat{x}_{e4}}{2\sqrt{2}} + \hat{x}_3^{(0)} e^{-r}, \\ \hat{x}_{D4} &= \frac{\hat{x}_{e4}}{\sqrt{2}} + \hat{x}_4^{(0)} e^{-r}, \\ \hat{p}_{D2} &= \frac{\hat{p}_{e4}}{2\sqrt{6}} + \hat{p}_2^{(0)} e^{-r},\end{aligned}\quad (17)$$

where \hat{x}_{D3} and \hat{x}_{D4} are out-of-phase. The corresponding output state is

$$\begin{aligned}\hat{x}_{out} &= \hat{x}_{in} - \frac{\hat{x}_{e4}}{\sqrt{3}}, \\ \hat{p}_{out} &= \hat{p}_{in} - \frac{\hat{p}_{e4}}{\sqrt{3}}.\end{aligned}\quad (18)$$

The measurement results of $\frac{\sqrt{2}}{\sqrt{3}}\hat{x}_{D4}$ and $2\sqrt{2}\hat{p}_{D2}$ should be fedforward to \hat{x}_{out} and \hat{p}_{out} to eliminate the error. The corrected output mode is

$$\begin{aligned}\hat{x}'_{out} &= \hat{x}_{in} + \frac{\sqrt{2}}{\sqrt{3}}\hat{x}_4^{(0)} e^{-r}, \\ \hat{p}'_{out} &= \hat{p}_{in} + 2\sqrt{2}\hat{p}_2^{(0)} e^{-r},\end{aligned}\quad (19)$$

and the corresponding noise powers are

$$\langle \Delta^2 \hat{x}'_{out} \rangle = \langle \Delta^2 \hat{x}_{in} \rangle + \frac{2}{3} \times \frac{1}{4} e^{-2r}, \quad (20)$$

and

$$\langle \Delta^2 \hat{p}'_{out} \rangle = \langle \Delta^2 \hat{p}_{in} \rangle + 8 \times \frac{1}{4} e^{-2r}, \quad (21)$$

respectively.

When the error is occurring in channel 5, we have non-zero syndrome measurements on

$$\begin{aligned}\hat{x}_{D3} &= \frac{\hat{x}_{e5}}{2\sqrt{2}} + \hat{x}_3^{(0)} e^{-r}, \\ \hat{x}_{D4} &= \frac{\hat{x}_{e5}}{\sqrt{2}} + \hat{x}_4^{(0)} e^{-r}, \\ \hat{p}_{D2} &= \frac{-\hat{p}_{e5}}{2\sqrt{6}} + \hat{p}_2^{(0)} e^{-r},\end{aligned}\quad (22)$$

where \hat{x}_{D3} and \hat{x}_{D4} are in-phase. The output state is

$$\begin{aligned}\hat{x}_{out} &= \hat{x}_{in} + \frac{\hat{x}_{e5}}{\sqrt{3}}, \\ \hat{p}_{out} &= \hat{p}_{in} + \frac{\hat{p}_{e5}}{\sqrt{3}}.\end{aligned}\quad (23)$$

By feedforwarding $\frac{-\sqrt{2}}{\sqrt{3}}\hat{x}_{D4}$ and $2\sqrt{2}\hat{p}_{D2}$ to \hat{x}_{out} and \hat{p}_{out} , the error will be corrected. The output mode after correction is

$$\begin{aligned}\hat{x}'_{out} &= \hat{x}_{in} - \frac{\sqrt{2}}{\sqrt{3}}\hat{x}_4^{(0)} e^{-r}, \\ \hat{p}'_{out} &= \hat{p}_{in} + 2\sqrt{2}\hat{p}_2^{(0)} e^{-r}\end{aligned}\quad (24)$$

and the corresponding noise powers are

$$\langle \Delta^2 \hat{x}'_{out} \rangle = \langle \Delta^2 \hat{x}_{in} \rangle + \frac{2}{3} \times \frac{1}{4} e^{-2r}, \quad (25)$$

and

$$\langle \Delta^2 \hat{p}'_{out} \rangle = \langle \Delta^2 \hat{p}_{in} \rangle + 8 \times \frac{1}{4} e^{-2r}, \quad (26)$$

respectively.

Table C1 The noise powers of the output state (with the unit of dB).

Error in channel	Quadrature of output	Noise of the output state without squeezing on ancilla modes	Noise of the output state with squeezing on ancilla modes
1	x	0.15 ± 0.30 (8.22 ± 0.31)	
	p	0.13 ± 0.30 (-2.78 ± 0.27)	
2	x	0.19 ± 0.29 (8.09 ± 0.31)	
	p	0.18 ± 0.30 (-2.73 ± 0.29)	
3	x	2.39 ± 0.28 (9.85 ± 0.27)	1.37 ± 0.29 (8.93 ± 0.27)
	p	4.80 ± 0.29 (4.28 ± 0.28)	3.07 ± 0.31 (1.46 ± 0.30)
4	x	2.47 ± 0.34 (9.96 ± 0.32)	1.49 ± 0.29 (8.89 ± 0.29)
	p	9.13 ± 0.30 (9.25 ± 0.27)	6.40 ± 0.28 (6.04 ± 0.30)
5	x	2.99 ± 0.31 (9.51 ± 0.27)	1.14 ± 0.28 (9.02 ± 0.30)
	p	9.01 ± 0.32 (9.03 ± 0.32)	5.94 ± 0.30 (6.10 ± 0.33)

The noise powers of the output state in and out of brackets are for the case of a squeezed and a vacuum state used as input state, respectively.

C. Noise power of the output state

The measured noise power of the output state in QEC is shown in table C1. Measurement frequency of noise

power is 2 MHz, the spectrum analyzer resolution bandwidth is 30 kHz, and the video bandwidth is 300 Hz.

-
- [1] M. A. Nielsen and I. L. Chuang, *Quantum Computation And Quantum Information*. (Cambridge University Press, 2000).
- [2] P. W. Shor, Phys. Rev. A. **52**, R2493-R2496 (1995).
- [3] R. Laflamme, C. Miquel, J. P. Paz, and W. H. Zurek, Phys. Rev. Lett. **77**, 198-202 (1996).
- [4] E. Dennis, A. Landahl, A. Kitaev, and J. Preskill, J. Math. Phys. **43**, 4452-4505 (2002).
- [5] A. G. Fowler, M. Mariantoni, J. M. Martinis, and A. N. Cleland, Phys. Rev. A **86**, 032324 (2012).
- [6] D. G. Cory, M. D. Price, W. Maas, E. Knill, R. Laflamme, W. H. Zurek, T. F. Havel, and S. S. Somaroo, Phys. Rev. Lett. **81**, 2152-2155 (1998).
- [7] E. Knill, R. Laflamme, R. Martinez, and C. Negrevergne, Phys. Rev. Lett. **86**, 5811-5814 (2001).
- [8] N. Boulant, L. Viola, E. M. Fortunato, and D. G. Cory, Phys. Rev. Lett. **94**, 130501 (2005).
- [9] J. Chiaverini, D. Leibfried, T. Schaetz, M. D. Barrett, R. B. Blakestad, J. Britton, W. M. Itano, J. D. Jost, E. Knill, C. Langer, R. Ozeri and D. J. Wineland, Nature **432**, 602-605 (2004).
- [10] P. Schindler, J. T. Barreiro, T. Monz, V. Nebendahl, D. Nigg, M. Chwalla, M. Hennrich, and R. Blatt, Science **332**, 1059-1061 (2011).
- [11] X.-C. Yao, T.-X. Wang, H.-Z. Chen, W.-B. Gao, A. G. Fowler, R. Raussendorf, Z.-B. Chen, N.-L. Liu, C.-Y. Lu, Y.-J. Deng, Y.-A. Chen and J.-W. Pan, Nature **482**, 489-494 (2012).
- [12] B. A. Bell, D. A. Herrera-Martí M. S. Tame, D. Markham, W. J. Wadsworth and J. G. Rarity, Nat. Commun. **5**, 3658 (2014).
- [13] M. D. Reed, L. DiCarlo, S. E. Nigg, L. Sun, L. Frunzio, S. M. Girvin and R. J. Schoelkopf, Nature **482**, 382-385 (2012).
- [14] R. Barends, et al. Nature **508**, 500-503 (2014).
- [15] C. Ottaviani, and D. Vitali, Phys. Rev. A **82**, 012319 (2010).
- [16] S. L. Braunstein and P. van Loock, Rev. Mod. Phys. **77**, 513-577 (2005).
- [17] C. Weedbrook, S. Pirandola, R. García-Patrón, N. J. Cerf, T. C. Ralph, J. H. Shapiro, and S. Lloyd, Rev. Mod. Phys. **84**, 621-669 (2012).
- [18] A. Furusawa, J. L. Sørensen, S. L. Braunstein, C. A. Fuchs, H. J. Kimble, and E. S. Polzik, Science **282**, 706-709 (1998).
- [19] X. Li, Q. Pan, J. Jing, J. Zhang, C. Xie, and K. Peng, Phys. Rev. Lett. **88**, 047904 (2002).
- [20] N. C. Menicucci, P. van Loock, M. Gu, C. Weedbrook, T. C. Ralph, and M. A. Nielsen, Phys. Rev. Lett. **97**, 110501 (2006).
- [21] M. Gu, C. Weedbrook, N. C. Menicucci, T. C. Ralph, and P. van Loock, Phys. Rev. A **79**, 062318 (2009).
- [22] R. Ukai, N. Iwata, Y. Shimokawa, S. C. Armstrong, A. Politi, J. I. Yoshikawa, P. van Loock, and A. Furusawa, Phys. Rev. Lett. **106**, 240504 (2011).
- [23] X. Su, S. Hao, X. Deng, L. Ma, M. Wang, X. Jia, C. Xie, and K. Peng, Nat. Commun. **4**, 2828 (2013).
- [24] S. L. Braunstein, Nature **394**, 47-49 (1998).
- [25] S. Lloyd and Jean-Jacques E. Slotine, Phys. Rev. Lett. **80**, 4088-4091 (1998).
- [26] S. L. Braunstein, Phys. Rev. Lett. **80**, 4084-4087 (1998).
- [27] T. A. Walker and S. L. Braunstein, Phys. Rev. A **81**, 062305 (2010).
- [28] M. M. Wilde, H. Krovi, and T. A. Brun, Phys. Rev. A **76**, 052308 (2007).
- [29] J. Niset, U. L. Andersen, and N. J. Cerf, Phys. Rev. Lett.

- 101**, 130503 (2008).
- [30] T. C. Ralph, *Phys. Rev. A* **84**, 022339 (2011).
 - [31] T. Aoki, G. Takahashi, T. Kajiya, J. Yoshikawa, S. L. Braunstein, P. van Loock and A. Furusawa, *Nat. Phys.* **5**, 541-546 (2009).
 - [32] M. Lassen, M. Sabuncu, A. Huck, J. Niset, G. Leuchs, N. J. Cerf and U. L. Andersen, *Nat. Photon.* **4**, 700-705 (2010).
 - [33] M. Lassen, A. Berni, L. S. Madsen, R. Filip, and U. L. Andersen, *Phys. Rev. Lett.* **111**, 180502 (2013).
 - [34] J. Niset, J. Fiurášek, and N. J. Cerf, *Phys. Rev. Lett.* **102**, 120501 (2009).
 - [35] J. Heersink, C. Marquardt, R. Dong, R. Filip, S. Lorenz, G. Leuchs, and U. L. Andersen, *Phys. Rev. Lett.* **96**, 253601 (2006).
 - [36] R. Dong, M. Lassen, J. Heersink, C. Marquardt, R. Filip, G. Leuchs and U. L. Andersen, *Nat. Phys.* **4**, 919-923 (2008).
 - [37] B. Hage, A. Samblowski, J. DiGuglielmo, A. Franzen, J. Fiurášek and R. Schnabel, *Nat. Phys.* **4**, 915-918 (2008).
 - [38] P. van Loock, *J. Mod. Opt.* **57**, 1965-1971 (2010).
 - [39] J. Zhang, and S. L. Braunstein, *Phys. Rev. A* **73**, 032318 (2006).
 - [40] P. van Loock, C. Weedbrook, and M. Gu, *Phys. Rev. A* **76**, 032321 (2007).
 - [41] P. van Loock, and A. Furusawa, *Phys. Rev. A* **67**, 052315 (2003).
 - [42] H. Nha, and H. J. Carmichael, *Phys. Rev. A* **71**, 032336 (2005).
 - [43] H. Scutaru, *J. Phys. A* **31**, 3659 (1998).
 - [44] Y. Wang, Y. Zheng, C. Xie, and K. Peng, *IEEE J. Quantum Electronics* **47**, 1006-1013 (2011).
 - [45] Y. Wang, H. Shen, X. Jin, X. Su, C. Xie, and K. Peng, *Opt. Express* **18**, 6149-6155 (2010).
 - [46] Y. Zhang, H. Wang, X. Li, J. Jing, C. Xie, and K. Peng, *Phys. Rev. A* **62**, 023813 (2000).